

Check for updates

www.chemeurj.org

Tuning the Topology of Two-Dimensional Covalent Organic Frameworks through Site-Selective Synthetic Strategy

Xueying Wu,^[a] Xihao Tang,^[a] Kai Zhang,^[a] Chelsea Harrod,^[b] Rui Li,^[a] Jialin Wu,^[a] Xi Yang,^[a] Shengrun Zheng,*^[a, c] Jun Fan,^[a, c] Weiguang Zhang,^[a, c] Xinle Li,*^[b] and Songliang Cai*^[a, c]

Tuning the topology of two-dimensional (2D) covalent organic frameworks (COFs) is of paramount scientific interest but remains largely unexplored. Herein, we present a site-selective synthetic strategy that enables the tuning of 2D COF topology by simply adjusting the molar ratio of an amine-functionalized dihydrazide monomer (NH₂-Ah) and 4,4',4"-(1,3,5-triazine-2,4,6-triyl)tribenzaldehyde (Tz). This approach resulted in the formation of two distinct COFs: a clover-like 2D COF with free amine groups (NH₂-Ah-Tz) and a honeycomb-like COF without amine groups (Ah-Tz). Both COFs exhibited good crystallinity and moderate porosity. Remarkably, the clover-shaped

NH₂–Ah–Tz COF, with abundant free amine groups, displayed significantly enhanced adsorption capacities toward crystal violet (CV, 261 mg/g) and congo red (CR, 1560 mg/g) compared to the non-functionalized honeycomb-like Ah–Tz COF (123 mg/g for CV and 1340 mg/g for CR), underscoring the pivotal role of free amine functional groups in enhancing adsorption capacities for organic dyes. This work highlights that the site-selective synthetic strategy paves a new avenue for manipulating 2D COF topology by adjusting the monomer feeding ratio, thereby modulating their adsorption performances toward organic dyes.

Introduction

Covalent organic frameworks (COFs) are an emerging class of crystalline porous polymers formed by the precise linking of organic monomers via strong covalent bonds. COFs possess nontrivial structural attributes, such as low density, high crystallinity, large specific surface area, superb chemical stability, adjustable poremetrics, and customizable skeletons.^[1-5] Consequently, COFs hold immense promise across a wide spectrum of applications spanning gas storage, [6-8] chromatographic separation, [9-13] heterogeneous catalysis, [14-18] chemical sensing, [19-23] optoelectronics, [24-26] and energy storage, [27-30] Among these diverse applications, there has been a growing interest in recent years in the use of COF adsorbents with task-specific affinity sites for the removal of aqueous pollutants. Of particular interest, amine-functionalized COFs have demon-

strated extraordinary efficacy in selectively removing environmentally harmful pollutants.[31-36] To date, four strategies have been established for constructing amine-functionalized COFs. The first strategy involves the post-synthetic reduction of existing COFs.[36,37] For instance, the reduction of nitro groups in pre-formed COFs results in the formation of amine-functionalized COFs.[37] The second approach is the monomer exchange strategy, wherein COF monomers are exchanged with those bearing multiple amine groups.[38-40] However, this process often requires a lengthy exchange reaction time and can lead to challenges in retaining the pristine COF crystallinity after monomer exchange. The third method is sub-stoichiometric synthesis, which might generate unpredictable defects due to the identical reactivity of the amine groups of the monomers used for constructing imine-linked COFs.[41-43] The fourth method, proposed by our group in 2021, is the site-selective synthetic strategy. This approach is simple to execute and yields targeted COFs in a single reaction step.[35,44,45] It leverages the different reactivities of amine and hydrazide with aldehyde to produce amine-functionalized 2D COFs, exclusively giving rise to honeycomb-like COFs to date.

On the other hand, the structural topology of 2D COFs is intricately controlled through the deliberate selection of rigid building blocks with different symmetries. 2D COFs harness the rigidity of their constituent monomers, each possessing reactive sites arranged in a particular geometry. This geometric alignment serves as a blueprint for the growth of polygonal frameworks, resulting in a diverse array of topologies, including trigonal, tetragonal, rhombic, hexagonal, and Kagome shapes. [2] Given that COF topologies can lead to intriguing material properties and contribute to the advancement of reticular chemistry, there have been a few studies on the topology modulation of 2D COFs in recent years. For instance, in 2017, Zhao's group demonstrated the capability to switch 2D COFs

GDMPA Key Laboratory for Process Control and Quality Evaluation of Chiral Pharmaceuticals, and Guangzhou Key Laboratory of Analytical Chemistry for Biomedicine

School of Chemistry, South China Normal University Guangzhou, 510006 (China) E-mail: songliangcai@m.scnu.edu.cn Zhenqsr@cnu.edu.cn

[b] C. Harrod, Prof. X. Li Department of Chemistry Clark Atlanta University Atlanta, Georgia, 30314 (United States) E-mail: xli1@cau.edu

[c] Prof. S. Zheng, Prof. J. Fan, Prof. W. Zhang, Prof. S. Cai Guangdong Longsmall Biochemical Technology Co. Ltd. Qingyuan, 511517 (China)

Supporting information for this article is available on the WWW under https://doi.org/10.1002/chem.202303781

[[]a] X. Wu, X. Tang, K. Zhang, R. Li, J. Wu, X. Yang, Prof. S. Zheng, Prof. J. Fan, Prof. W. Zhang, Prof. S. Cai

Chemistry Europe ropean Chemical

between orthorhombic and hexagonal topologies by introducing alkyl substituents to a monomer.[46] Wang's group exerted control over the rhombic and Kagome topologies of on-surfacesynthesized 2D COFs by varying the monomer concentrations.[47] In 2021, Chen's group employed a "two-inone" strategy to create highly crystalline 2D COFs, and their topologies were fine-tuned by adjusting either the solvents or the monomer concentrations.[48] Despite notable progress, manipulating the 2D COF topology using the same monomer combination has been rarely reported.

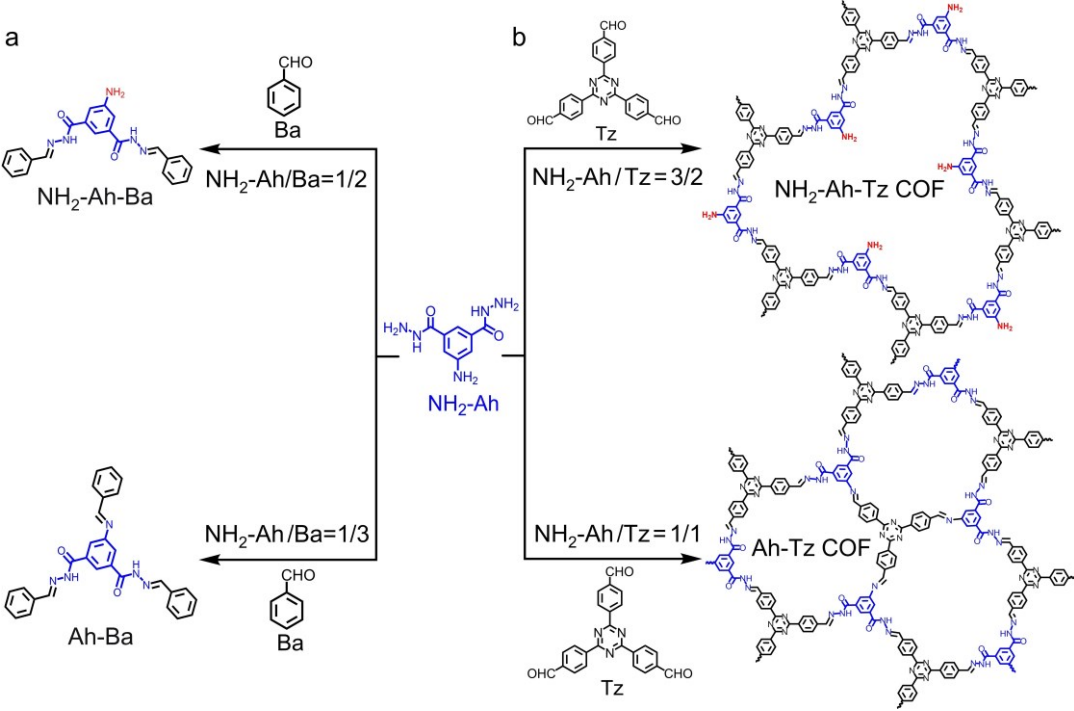
In this study, we introduce a site-selective synthetic strategy that facilely modulates the topology of 2D COFs by adjusting the molar ratio between an amine-containing dihydrazine (NH_2-Ah) and 4,4',4"-(1,3,5-triazine-2,4,6monomer triyl)tribenzaldehyde (Tz). The condensation of NH₂-Ah with Tz in a molar ratio of 3/2 led to the site-selective synthesis of a clover-shaped NH₂-Ah-Tz COF with free amine groups, while the reaction of NH₂-Ah with Tz in a molar ratio of 1/1 gave rise to a honeycomb-like Ah-Tz COF without amine groups. When applied for the selective removal of aqueous organic dye pollutants, the clover-shaped NH2-Ah-Tz COF containing amine functional groups exhibited largely enhanced adsorption abilities, in comparison to those of the honeycomb-like Ah-Tz COF without amine groups.

Results and Discussion

Synthesis and characterization of NH2 Ah Iz and Ah Iz COFs

We commenced our study with the synthesis of two molecular model compounds, NH₂-Ah-Ba and Ah-Ba, by adjusting the feed ratio between amine-functionalized dihydrazide (NH₂-Ah) and benzaldehyde (Ba). At an NH₂-Ah/Ba molar ratio of 1/3, a grayish-white solid of NH2-Ah-Ba was obtained with a yield of 78 %. In contrast, at an NH₂-Ah/Ba molar ratio of 1/2, a white solid of Ah-Ba was obtained with a yield of 84 % (Scheme 1a). The structures of these two model compounds were unambiguously confirmed by ¹H NMR, ¹³C NMR, and LC-MS analyses (see supporting information). The molecular model system demonstrates that the selective retention of unreacted amine groups can be achieved by varying the monomer feed ratio, highlighting the exceptional efficiency of our site-selective synthetic strategy. Encouraged by this result from the model compound, we applied it to the synthesis of two new 2D COFs, namely NH₂-Ah-Tz COF and Ah-Tz COF. These COFs were synthesized solvothermally via the Schiff-base reaction of 4,4',4"-(1,3,5triazine-2,4,6-triyl)tribenzaldehyde (Tz) and amine-functionalized dihydrazide (NH₂-Ah) at different molar ratios (Scheme 1b). The synthesis was conducted in o-dichlorobenzene/ethanol, catalyzed by 6 M acetic acid, and maintained at 110 °C for 3 days. NH₂-Ah-Tz COF was obtained as a dark yellow solid in high yields by the condensation of NH2-Ah with Tz at a molar ratio of 3/2, while Ah-Tz COF was obtained as a bright yellow solid by the reaction of NH_2 -Ah with Tz at a molar ratio of 1/1. Elemental analyses were conducted for both NH₂-Ah-Tz

and Ah-Tz COFs, and the results were given in Table S1. The



Scheme 1. (a) Synthesis of the model compounds NH₂-Ah-Ba and Ah-Ba. (b) Synthesis of NH₂-Ah-Tz and Ah-Tz COFs.

measured C and N contents of NH₂-Ah-Tz COF and Ah-Tz COF were found to be lower than the theoretical values, which might be due to the challenging removal of the guest molecules in the pore channels of the resulting COFs. It was worth noting that the N/C ratio of NH₂-Ah-Tz COF (1/2.99) was much higher than that of Ah-Tz COF (1/3.83), which was attributed to the greater nitrogen content in the aminefunctionalized NH2-Ah-Tz COF. The crystalline structures of NH₂-Ah-Tz and Ah-Tz COFs were verified by X-ray powder diffraction (PXRD) analysis. As illustrated in Figure 1a, the diffraction pattern of NH2-Ah-Tz COF exhibited an intense peak at 5.0° and three minor peaks at 8.6°, 13.1° and 26.3°. In contrast, Ah-Tz COF displayed a strong diffraction peak at around 5.0°, accompanied by four minor peaks at 8.5°, 13.1°, 15.2° and 26.2° (Figure 1e). A comparison of the experimental PXRD pattern with the simulated one revealed that NH₂-Ah-Tz COF adopted a clover-like 2D network with ABC packing (Figures 1a, 1d, and Table S4), as opposed to AA packing (Figure 1b and Table S2) and AB packing (Figure 1c and Table S3). Such an amine-functionalized NH2-Ah-Tz COF with ABC stacking mode was similar to those of the other reported clover-like COFs.[49-51] Likewise, the packing mode of Ah-Tz COF closely resembled that of NH2-Ah-Tz COF. This was evident from the fact that the experimental PXRD pattern of Ah-Tz COF matched well with the simulated pattern generated from the ABC packing mode, rather than the AA packing and AB packing modes (Figures 1e-1 h and Tables S5-S7). The ABC stacking mode of Ah-Tz COF was similar to those of the previously reported honeycomb-like COFs.[52-54] The suggested ABC packing modes were therefore utilized for the Pawley refinements for NH₂-Ah-Tz and Ah-Tz COFs, producing the PXRD patterns

which were very close to their corresponding experimental ones (Figure S1). The final agreement factors of R_p and R_{wp} were found to be 3.42%, 2.68% for NH₂–Ah–Tz COF, and 2.40%, 1.89% for Ah–Tz COF, respectively. Notably, this work represents the first attempt at creating a clover-like COF through the site-selective synthetic strategy. Furthermore, it stands as the first example of tuning 2D COF topology through the straightforward variation of the molar ratio of two monomers.

Fourier transform infrared (FT-IR) studies were conducted to further validate the successful synthesis of two COFs. As shown in Figure 2a, the FT-IR spectra of both NH₂-Ah-Tz COF and Ah-Tz COF revealed the absence of aldehyde stretching vibrations (1706 cm⁻¹) and the emergence of characteristic C=N peaks (~1610 cm⁻¹), confirming the imine formation. These C=N stretching bands were in close agreement with those observed in the model compounds of NH₂-Ah-Ba (1616 cm⁻¹) and Ah-Ba (1607 cm⁻¹) (Figure S2). Moreover, in the FT-IR spectrum of Ah-Tz COF, the amine vibration bands disappeared in comparison to those observed in the NH₂-Ah monomer (3200-3450 cm⁻¹). Noteworthy, some characteristic amine stretching peaks (3221 and 3418 cm⁻¹) were still evident in the FT-IR spectrum of NH₂-Ah-Tz COF, indicating the presence of free amine functional group in NH2-Ah-Tz COF, whereas these groups were absent in Ah-Tz COF. Similar amine characteristic bands were also found in the FT-IR spectrum of the model compound NH₂-Ah-Ba (Figure S2). The presence of free amine groups was further corroborated by X-ray photoelectron spectroscopy (XPS) analysis. The N 1s spectrum of NH₂-Ah-Tz COF exhibited four peaks centered at 398.31 eV, 399.34 eV, 400.23 eV, and 401.55 eV, corresponding to the N atoms of C=N from the hydrazone unit, C=N from the triazine ring, C-N bond

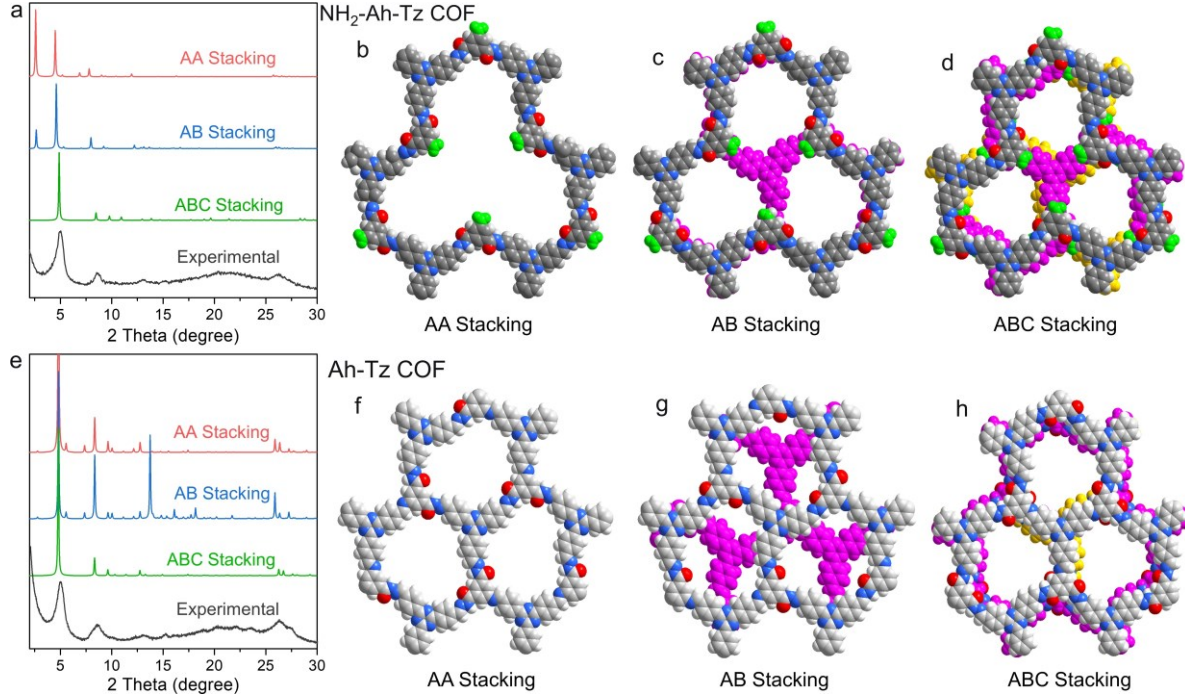


Figure 1. (a) Experimental and simulated PXRD patterns of NH₂ Ah Tz COF; (b–d) Simulated structures of NH₂ Ah Tz COF with AA, AB, and ABC stacking modes, respectively; (e) Experimental and simulated PXRD patterns of Ah Tz COF; (f–h) Simulated structures of Ah Tz COF with AA, AB and ABC stacking modes.

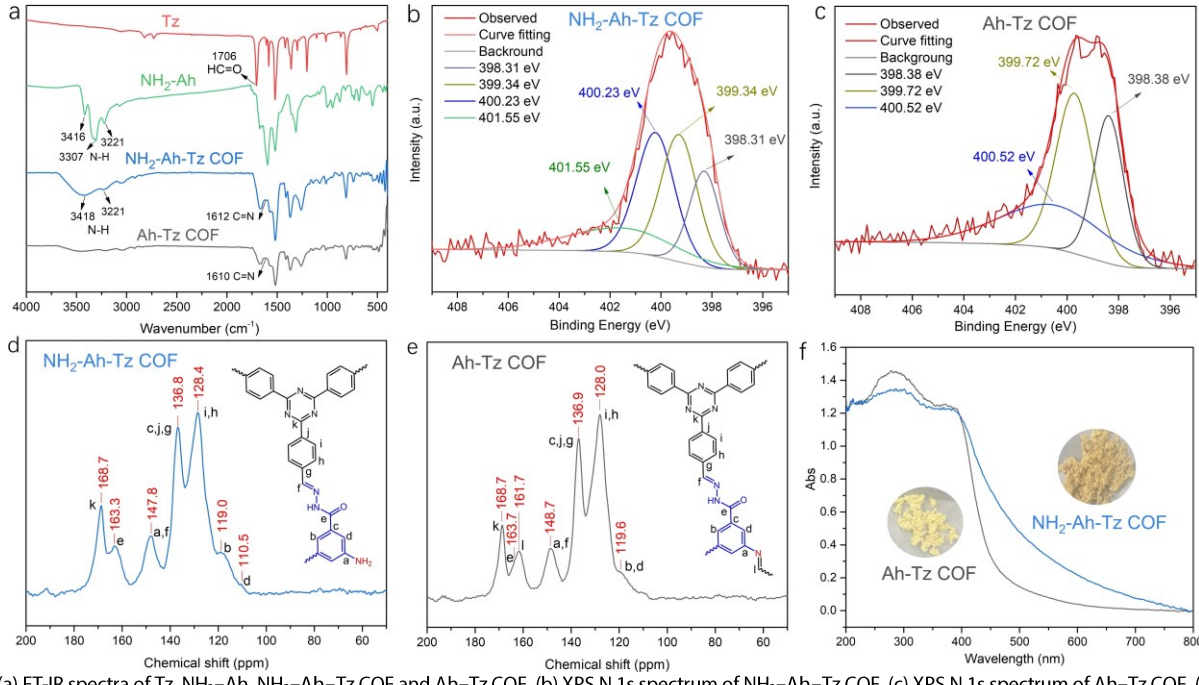


Figure 2. (a) FT-IR spectra of Tz, NH₂-Ah, NH₂-Ah-Tz COF and Ah-Tz COF. (b) XPS N 1s spectrum of NH₂-Ah-Tz COF. (c) XPS N 1s spectrum of Ah-Tz COF. Solid-state ¹³C CP-MAS NMR spectrum of NH₂-Ah-Tz COF. (e) Solid-state ¹³C CP-MAS NMR spectrum of Ah-Tz COF. (f) Solid UV absorption spectra of NH₂-Ah-Tz COF and Ah-Tz COF.

and the -NH₂ group, respectively (Figure 2b). By comparison, the N 1s spectrum of Ah-Tz COF only displayed three peaks at 398.38 eV, 399.72 eV, and 400.52 eV, which were attributed to the C=N from the hydrazone bond, C=N from the triazine ring and the C-N bond, respectively (Figure 2c). Solid-state ¹³C crosspolarization magic angle spinning (CP-MAS) NMR spectra of NH₂-Ah-Tz COF and Ah-Tz COF exhibited resonance signals at 147.8 and 148.7 ppm, which were characteristics of the C=N carbons in the hydrazone linkages and aromatic carbons connected to the free or reacted -NH2 groups (Figures 2d, 2e and S3a). More importantly, the signal at 161.7 ppm in the ¹³C CP-MAS NMR spectrum of Ah_Tz COF could be ascribed to the carbons of imine linkage,[55] which was absent in that of NH₂-Ah-Tz COF. These results were in good consistency with the ¹³C NMR spectra of the corresponding model compounds NH₂-Ah-Ba and Ah-Ba (Figure S3b).

Thermogravimetric analysis (TGA) showed that both NH2-Ah-Tz COF and Ah-Tz COF displayed high thermal stability, exhibiting a slight weight loss before the temperature of 365°C in a nitrogen atmosphere (Figure S4). Solid UV-vis absorption spectra demonstrated that NH2-Ah-Tz COF exhibited a broader UV absorption range than that of Ah-Tz COF. This observation was consistent with the visual appearance of the powders, as NH₂-Ah-Tz COF was darker than Ah-Tz COF (Figure 2f). Moreover, the bandgap of NH2-Ah-Tz COF was determined to be 2.67 eV, which was smaller than that of Ah-Tz COF (2.84 eV), as presented in Figure S5. Scanning electron microscopy (SEM) micrographs of the two COFs presented rod-shaped morphologies with different lengths (Figures S6 and S7). The nitrogen adsorption-desorption isotherms of both COFs demonstrated a Type IV behavior,

indicative of their microporous character (Figures 3a and 3b). The Brunauer-Emmett-Teller (BET) surface areas were calculated to be 119 m^2 g^{-1} for NH₂-Ah-Tz COF and 149 m^2 g^{-1} for Ah-Tz COF. The pore size distribution was estimated from nonlocal density functional theory (NLDFT), yielding pore sizes of 1.63 nm and 1.28 nm for NH2-Ah-Tz COF and Ah-Tz COF, respectively (Figures 3c and 3d). The relatively modest BET surface areas can be attributed to the unusual ABC stacking mode in both NH₂-Ah-Tz and Ah-Tz COFs, which has been

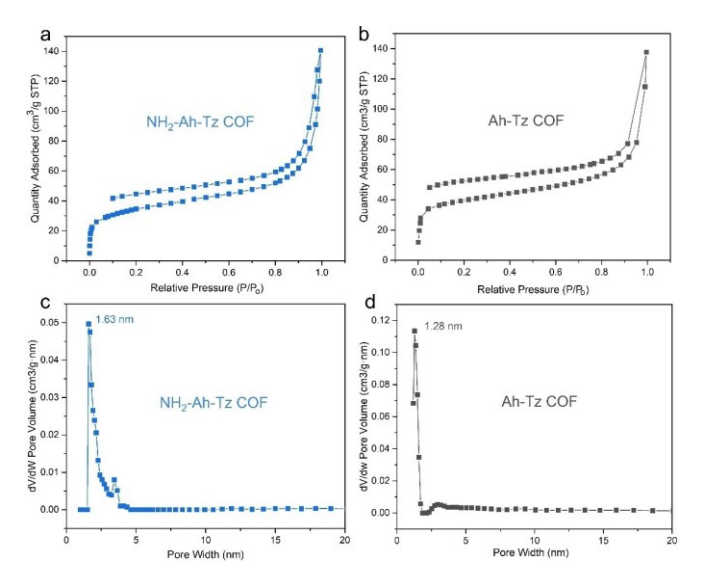


Figure 3. N₂ adsorption-desorption isotherm curves of (a) NH₂-Ah-Tz COF and (b) Ah-Tz COF at 77 K. The corresponding pore size distribution profile of (c) NH₂-Ah-Tz COF and (d) Ah-Tz COF.

observed in prior studies.^[49-54] The chemical stabilities of NH₂-Ah-Tz COF and Ah-Tz COF were assessed by soaking the COF samples in different solvents at room temperature for 48 hours. It was found that both NH₂-Ah-Tz and Ah-Tz COFs were stable in dichloromethane (DCM), N,N-dimethylformamide (DMF), tetrahydrofuran (THF), water, aqueous NaOH (1 M) and HCl (1 M), as evidenced by only slight changes in their PXRD patterns after solvent treatment (Figure S8). The good chemical stabilities of both NH₂-Ah-Tz and Ah-Tz COFs could be attributed to the robust hydrazone linkages in the resulting COFs.^[19,56]

Dye adsorption isotherms

With both COFs thoroughly characterized, we sought to assess their potential in the selective removal of aqueous organic dye pollutants. The dye absorption capacities of COFs as adsorbents were determined by measuring the adsorption isotherms of crystal violet (CV) and congo red (CR) organic dyes (Figure 4a and Table S8). The equilibrium data were analyzed and fitted with Langmuir, Freundlich, and Temkin isothermal adsorption models to elucidate the interactions between COFs and two dye molecules. As illustrated in Figure 4b, NH2-Ah-Tz COF exhibited a maximum adsorption capacity of 261 mg/g towards CV, surpassing the non-functionalized Ah-Tz COF (123 mg/g) by 2.1-fold. As for CR, both NH₂-Ah-Tz COF and Ah-Tz COF displayed high adsorption capacities, reaching up to 1560 mg/g and 1340 mg/g, respectively (Figure 4c). The amine-functionalized clover-shaped NH2-Ah-Tz COF demonstrated significantly enhanced adsorption capacities for both CV and CR compared to the non-functionalized honeycomb-like Ah-Tz COF. This underscores the effectiveness of introducing amine functional groups into COF structures for improving their adsorption abilities towards organic dyes. The amine groups in NH₂-Ah-Tz COF are prone to forming hydrogen bonds with dye molecules, resulting in higher maximum adsorption capacities of $NH_2\text{--}Ah\text{--}Tz$ COF for two organic dyes. $^{\![31,32]}$ To underline the outstanding performance of NH₂-Ah-Tz COF, we compared the

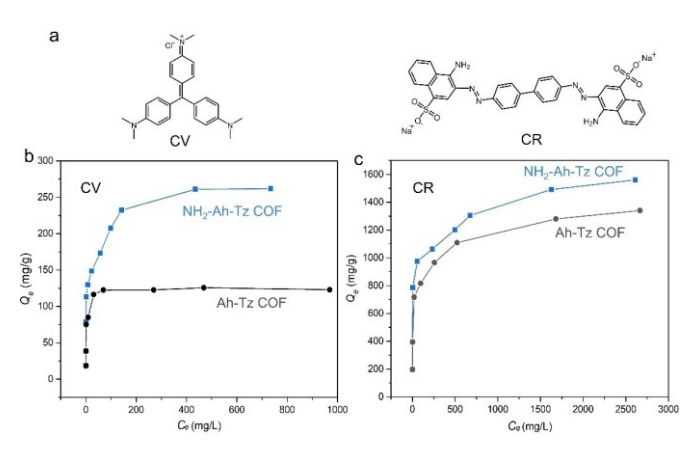


Figure 4. (a) The structures of CV and CR organic dyes. (b) The adsorption isotherms of NH_2 -Ah-Tz COF and Ah-Tz COF for CV. (c) The adsorption isotherms of NH_2 -Ah-Tz COF and Ah-Tz COF for CR.

maximum adsorption capacities with those of reported adsorbents for CV and CR in Tables S9 and S10. The maximum adsorption capacity of NH₂-Ah-Tz COF for CR surpassed that of many reported metal-organic frameworks (MOFs) and COFs, such as Mn-UiO-66@GO-NH₂ (1265.82 mg/g),^[57] MIL-88 A(Fe) (PMFe-x) (1141.4 mg/g),^[58] COF-COONi/Ca (781.25/704.23 mg/ a),^[59] (234.4 mg/g),^[60] Fe₃O₄@MIL-53(AI) Fe₃O₄@TpPDA (179.4 mg/g),^[61] and so on. Similarly, the saturated adsorption capacity of NH₂-Ah-Tz COF for CV was superior to many reported materials, such as SCNU-Z2 (847.4 mg/g),^[62] TpPa-SO₃Na COF (728.4 mg/g),^[63] COF-H2 (151.8 mg/g),^[64] COF-TPDD-COOH (88.02 mg/g),^[65] LYU-2 (44.8 mg/g)^[66] and Zn-MOF (7.355 mg/g)^[67] etc. The adsorption of NH₂-Ah-Tz COF and Ah-Tz COF on the two dye molecules conformed to the Langmuir isothermal adsorption model, indicating monolayer adsorption of CV and CR molecules on NH2-Ah-Tz COF and Ah-Tz COF (Figures S9 and S10).

Dye adsorption kinetics

The adsorption kinetics of NH₂-Ah-Tz COF and Ah-Tz COF for CV (20 mg/L) and CR (200 mg/L) were investigated. The amine-functionalized clover-like NH₂-Ah-Tz COF displayed much higher adsorption rates for CV and CR than those of the honeycomb-like Ah-Tz COF without amine groups (Figure 5). For NH₂-Ah-Tz COF, the removal rate of CV reached 97.1 % after 180 minutes of adsorption, while Ah-Tz COF achieved only 86.8% removal of CV in the same time frame. Moreover, the removal rate of CR by NH₂-Ah-Tz COF was 82.9 % at 300 minutes, significantly higher than the 71.8 % removal rate attained by Ah-Tz COF for CR. In addition, the aqueous solutions treated with NH₂-Ah-Tz COF exhibited a noticeably lighter color compared to those treated with Ah-Tz COF,

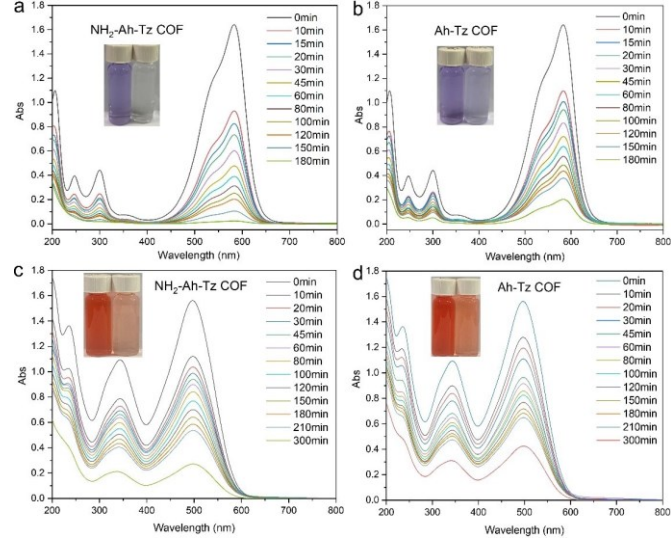


Figure 5. UV-Vis absorption spectra of CV treated with (a) NH_2 Ah Tz COF and (b) Ah—Tz COF at different times. UV-Vis absorption spectra of CR treated with (c) NH_2 —Ah—Tz COF and (d) Ah Tz COF at different times. The inset images present the corresponding color changes before (left) and after (right) the dye adsorption.

providing further evidence of the faster adsorption kinetics of NH₂-Ah-Tz COF than Ah-Tz COF. Although the adsorption rates of NH2-Ah-Tz COF for organic dyes were slower than those of the β-ketoenamine-linked COFs, [68,69] it was noteworthy that the maximum adsorption capacities of NH2-Ah-Tz COF toward CV and CR were superior to many reported MOF and COF-based materials, [57-67] rendering it still a promising adsorbent for the effective removal of dye pollutants from water. The adsorption kinetics of CV and CR on the two COFs were studied by quasi-first-order and quasi-second-order equations. The results indicated that the fitting data of the adsorption of CV by Ah-Tz COF conformed to the pseudo-first-order equation, and the other fitting results conformed to the pseudo-second-order equation (Figures S11 and S12). This suggested that the adsorption of CV by Ah-Tz COF was more likely to be physical adsorption.

Adsorption mechanism

To probe the molecular interactions between COFs and the adsorbed dyes, FT-IR studies were performed and the results were presented in Figure 6. The FT-IR spectra of NH₂-Ah-Tz COF and Ah-Tz COF exhibited prominent peaks at 1572 and 1574 cm⁻¹, corresponding to the C=C vibration in the benzene ring. Upon adsorption of CV, the FT-IR spectrum of NH₂-Ah-Tz COF@CV displayed characteristic peaks of CV at 1296 cm⁻¹ and 1172 cm⁻¹. Notably, the characteristic C=C peak shifted to 1585 cm⁻¹ compared to that of the pristine NH₂-Ah-Tz COF. In the case of Ah-Tz COF@CV, the FT-IR spectrum displayed characteristic peaks of CV at 1296 cm⁻¹ and 1272 cm⁻¹, with a similar shift in the aromatic C=C peaks to 1582 cm⁻¹ following adsorption. When CR was adsorbed, characteristic CR peaks

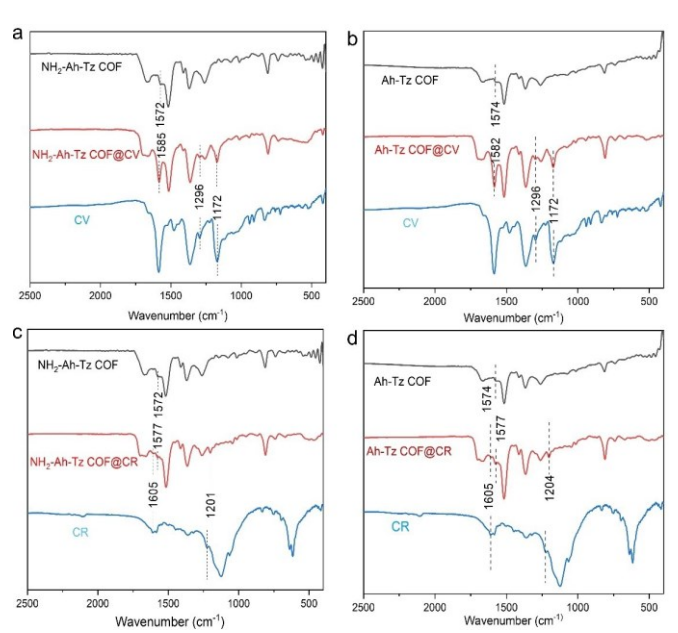


Figure 6. FT-IR spectra of (a) NH₂-Ah-TzCOF, CV and NH₂-Ah-TzCOF@CV.

NH2-ATZ-FDEOFWARK (A) ATZ-FDEOF, KASINULARALZ-TOFOER Rand

emerged at 1605 cm⁻¹ and 1201 cm⁻¹, 1605 cm⁻¹, and 1204 cm⁻¹ in the FT-IR spectra of NH₂–Ah–Tz COF@CR and Ah–Tz COF@CR, respectively. In both cases, the aromatic C=C stretching peaks shifted to 1577 cm⁻¹, indicating π - π interactions between the COF skeleton and the conjugated structure of the organic dye.^[70]

The significantly improved adsorption performance of NH₂-Ah-Tz COF compared to the non-functionalized Ah-Tz COF can be attributed to two primary factors. Firstly, the presence of free amine groups enables interactions with organic dyes through hydrogen bonds, such as N-H---N and N-H...O interactions, thereby enhancing the adsorption of organic dyes. Secondly, the disparity in pore sizes between the two COFs plays a crucial role. The molecular size of CV (1.39 nm×1.40 nm×0.40 nm) was slightly larger than the pore size of Ah-Tz COF (1.28 nm), making it challenging for CV to enter the pore channels of Ah-Tz COF. On the contrary, the pore size of Ah-Tz COF (1.63 nm) exceeds the molecular dimensions of CV, facilitating easy access for CV dye into the pore structure of NH2-Ah-Tz COF. This difference also contributes to the higher adsorption capacity and faster adsorption kinetic of NH₂-Ah-Tz COF than Ah-Tz COF for CV. Regarding CR, which has a linear structure with a molecular size of 2.36 nm×0.82 nm×0.50 nm, the pore channels of both NH₂-Ah-Tz and Ah-Tz COFs can be readily accessed. This accounts for the high adsorption capacities of both COFs towards CR.

Conclusions

In summary, we have demonstrated for the first time that the site-selective synthetic strategy provides a facile means to finetune the 2D COF topology. By adjusting the molar ratios of an amine-functionalized dihydrazide monomer (NH2-Ah) and Tz under solvothermal conditions, we synthesized a clover-like NH2-Ah-Tz COF with amine functional groups and a honevcomb-like Ah-Tz COF without amine functional groups. When employed as adsorbents for the removal of aqueous dye removal, NH2-Ah-Tz COF, enriched with amine functional groups, exhibited exceptional adsorption performance toward CV and CR, far exceeding that of the honeycomb-like Ah-Tz COF without amine group. The enhanced adsorption performance of NH2-Ah-Tz COF can be attributed to the strong between the amine groups and the dyes, in addition to the enlarged pore size. The molecular interactions between the COFs and the adsorbed dyes were verified through FT-IR studies. This work underscores the immense potential of the site-selective synthetic strategy in tuning 2D COF topology, thereby regulating their dye absorption properties and offering possibilities for broader applications. We envision that the siteselective synthetic strategy can be applied to modulate the topology of other 2D COFs or even 3D COFs by selecting appropriate, versatile amine-functionalized hydrazide linkers. These potentials are currently under investigation in our laboratory.

Experimental Section

Synthesis of amine-functionalized dihydrazide (NH2-Ah)

Dimethyl 5-amino-isophthalate (209 mg, 1 mmol), 98 % hydrazine hydrate (900 μ L), and anhydrous ethanol (2 mL) were placed in a 10 mL microwave tube. The mixture was deoxygenated with liquid nitrogen freezing for 15 minutes and then reacted in an oil bath at 80 °C for 24 hours. After cooling down to room temperature, the powder was washed with anhydrous ethanol several times and then dried in a vacuum oven at 100 °C overnight to yield a gray solid, 5-amino-isophthalic dihydrazide (NH2_Ah). ¹H-NMR (600 MHz, DMSO- d_6) δ (ppm) = 9.47 (s, 2H), 7.32 (s, 1H), 7.09 (s, 2H), 5.42 (s, 2H), 4.45 (s, 4H). ¹³C-NMR (150 MHz, DMSO- d_6) δ (ppm) = 166.91, 149.24, 134.81, 115.31, 113.10. MS (LC-MS) for $C_8H_{11}N_5O_2$ (Calcd: 209.09): m/z= 208.28 [M-H]-.

Synthesis of NH₂_Ah Ba and Ah Ba (molecular model compounds)

NH₂-Ah (31 mg, 0.15 mmol), benzaldehyde (31 μ L, 0.30 mmol), and methanol (2 mL) were charged in a 10 mL microwave vial. The mixture was then degassed by three freeze-pump-thawing cycles and finally heated at 82 °C for 48 hours. Upon cooling to room temperature, the precipitate was collected by filtration, washed with methanol several times, and dried overnight under vacuum, giving rise to the model compound of NH₂_Ah_Ba as an off-white solid (45 mg, yield: 78%). ¹H-NMR (600 MHz, DMSO- d_6) δ (ppm) = 11.85 (s, 2H), 8.46 (s, 2H), 7.73 (d, J = 7_{12} 2 Hz, 4H), 7.55 (s, 1H), 7.51–7.36 (m, 6H), 7.25 (s, 2H), 5.64 (s, 2H). C-NMR (150 MHz, DMSO- d_6) δ (ppm) = 163.96, 149.60, 148.14, 135.08, 134.84, 130.56, 129.34, 127.58, 116.36, 114.12. MS (LC-MS) for C_{22} H₁₉N₅O₂ (Calcd: 385.42): m/z= 384.23 [M-H]⁻.

NH₂-Ah (21 mg, 0.1 mmol), benzaldehyde (31 μ L, 0.30 mmol), and methanol (2 mL) were placed in a 10 mL microwave vial. The vial was then degassed by three freeze-pump-thawing cycles and finally heated at 82 °C for 48 hours. Upon cooling to room temperature, the precipitate was collected by filtration, washed with methanol several times, and dried overnight under vacuum to obtain the model compound of Ah_Ba as a white solid (40 mg, yield: 84 %). ¹H-NMR (600 MHz, DMSO- d_6) δ (ppm) = 12.08 (s, 2H), 8.83 (s, 1H), 8.52 (s, 2H), 8.38 (s, 1H), 8.03 (s, 4H), 7.77 (d, J = 6.7 Hz, 4H), 7.59 (d, J = 7.2 Hz, 3H), 7.48 (t, J = 7.5 Hz, 6H). ¹³C-NMR (150 MHz, DMSO- d_6) δ (ppm) = 163.41, 162.67, 152.16, 148.82, 136.15, 135.31, 134.69, 132.52, 130.71, 129.47, 129.41, 129.36, 127.68, 125.06, 123.62. MS (LC-MS) for $C_{29}H_{23}N_5O_2$ (Calcd: 473.53): m/z = 472.17 [M-H]-.

Synthesis of NH₂-Ah-Tz and Ah-Tz COFs

A mixture of Tz (7.9 mg, 0.02 mmol), NH₂_Ah (6.3 mg, 0.03 mmol), o-dichlorobenzene and anhydrous ethanol (0.67 mL and 0.33 mL, respectively) was added into a 10 mL glass bottle and then sonicated for 10 minutes. Acetic acid (0.1 mL, 6 M) was added to the mixture and argon was bubbled for 10 minutes, after which the glass bottle was quickly sealed and heated at 110 °C for 3 days. The precipitate was filtered, collected, and then washed with tetrahydrofuran and methanol to obtain a dark yellow solid powder. The obtained powder was soaked in tetrahydrofuran and methanol solvents for 2 days, during which fresh tetrahydrofuran and methanol solvents were exchanged 3 times. The powder was collected by centrifuge and dried under vacuum to obtain a clovershaped COF containing amine functional groups (NH₂-Ah_Tz COF) in a yield of 80 %.

A mixture of Tz (7.9 mg, 0.02 mmol), NH₂—Ah (4.2 mg, 0.02 mmol), 0.67 mL o-dichlorobenzene and 0.33 mL anhydrous ethanol was added into a 10 mL glass bottle and then sonicated for 10 minutes. Then, acetic acid (0.1 mL, 6 M) was added to the mixture and argon was bubbled for 10 minutes, after which the glass bottle was quickly sealed and heated at 110 °C for 3 days. The precipitate was filtered and collected and then washed with tetrahydrofuran and methanol to obtain a bright yellow solid powder. The obtained powder was soaked in tetrahydrofuran and methanol solvents for 2 days, during which fresh tetrahydrofuran and methanol solvents were exchanged 3 times, respectively. The powder was collected by centrifuge and dried under vacuum to obtain a honeycomb-like COF without amine functional groups (Ah—Tz COF) in a yield of 78%.

Dye adsorption test

NH₂—Ah_Tz COF or Ah_Tz COF (2.5 mg) was immersed in 10 mL organic dyes aqueous solutions with different initial concentrations ranging from 50 to 2000 ppm and stirred at room temperature in the dark for 72 hours. Then the mixture was filtered by PES membranes with 0.22 μ m micropore to remove any adsorbent. The concentrations of organic dyes in an aqueous solution were characterized by a UV-visible spectrophotometer. The adsorption capacity (Q_e) and the capacity at giving time (Q_t) of NH₂-Ah_Tz COF or Ah_Tz COF for organic dyes were calculated by the following equations, respectively:

$$Q_{t} \frac{\sqrt{\delta}C_0 - C_t \flat}{m}$$

$$Q_e \frac{1}{4} \frac{V \delta C_0 - C_e \flat}{m}$$

Where C_0 and C_e (mg· L⁻¹) are the concentrations of dyes in aqueous solutions at the beginning and equilibrium times, respectively, V (mL) represents the volume of the aqueous dye solution, and m (g) is the mass of the NH₂–Ah–Tz COF or Ah–Tz COF sample.

The adsorption isotherm data were fitted using Langmuir, Freundlich, and Temkin adsorption models. The Langmuir adsorption model formula is:

$$\frac{Ce}{Qe} \frac{1}{4} \frac{1}{K_L Q_m} \frac{C_e}{Q_m}$$

and formula of the Freundlich adsorption model is:

$$lnQ_e \frac{1}{4} lnK_F p \frac{1}{n} lnC_e$$

and formula of the Temkin adsorption model is:

Qe 1/4 BlnA b BlnCe

Where $C_{\rm e}$ (mg· L⁻¹) is the equilibrium concentration of dyes in an aqueous solution, $Q_{\rm e}$ (mg· g⁻¹) is the equilibrium adsorption capacity, Q_m (mg· g⁻¹) is the maximum adsorption capacity. While K_L is the Langmuir constant, K_F is the Freundlich constant, 1/n is adsorption intensity, B is a factor related to the heat of adsorption, A is the equilibrium binding constant.

The kinetic adsorption studies were performed in a similar method. NH_2 -Ah-Tz COF or Ah-Tz COF (3.0 mg) was added into organic

Chemistry Europe

Chemistry—A European Journal

dyes aqueous solutions, and the concentration of dyes at the given time was determined. For the adsorption studies, NH2_Ah_Tz COF or Ah_Tz COF (3.0 mg) powder was added into 10 mL aqueous solutions of crystal violet (CV) and congo red (CR), and the concentration of dyes at the giving time was determined. The adsorption kinetic data were fitted with the pseudo-first-order and pseudo-secondary-order models, respectively, and their equations are as follows:

 $\ln \delta q_e - q_t$ $\ln \delta q_e - k_1 t$

$$\frac{t}{q_t} \frac{1}{\sqrt{4}} \frac{1}{k_2 q^2} \triangleright \frac{t}{q_e}$$

Where q_t and q_t (mg g-1) represent the uptake capacity at the equilibrium and giving time t (min), k_t and k_z represent the pseudofirst-order rate constant and pseudo-second-order rate constant, respectively.

Acknowledgements

We gratefully acknowledge the financial support from the National Natural Science Foundation of P. R. China (Grant Nos. 22171092, 92056113, and 22073032), the Natural Science Foundation of Guangdong Province (Grant 2021A1515010211) and the Science and Technology Planning Project of Qingyuan (Grant No. 2023KJJ013). C. H. and X. L. are grateful for the support from the U.S. National Science Foundation HBCU-UP-RIA program (Grant No. 2100360) and PREC program (Grant No. 2216807).

Conflict of Interests

The authors declare no conflict of interest.

Data Availability Statement

The data that support the findings of this study are available from the corresponding author upon reasonable request.

Keywords: covalent organic frameworks synthetic strategy · topology control · organic dye removal

- [1] A. P. Cote, A. I. Benin, N. W. Ockwig, M. O'Keeffe, A. J. Matzger, O. M. Yaghi, Science 2005, 310, 1166-1170.
- K. Geng, T. He, R.Y. Liu, S. Dalapati, T. K. Tan, Z.P. Li, S. H. Tao, Y. F. Gong, Q. H. Jiang, D. L. Jiang, Chem. Rev. 2020, 120, 8814-8933.
- [3] P. J. Waller, F. Gándara, O. M. Yaghi, Acc. Chem. Res. 2015, 48, 3053-
- [4] X. L. Li, S. L. Cai, B. Sun, C. Q. Yang, J. Zhang, Y. Liu, *Matter* 2020, 3, 1507.
- S. L. Cai, W. G. Zhang, R. N. Zuckermann, Z. T. Li, X. Zhao, Y. Liu, Adv. Mater. 2015, 27, 5762.
- X. M. Liu, G. J. H. Lim, Y. X. Wang, L. Zhang, D. Mullangi, Y. Wu, D. Zhao, J. Ding, A. K. Cheetham, J. Wang, Chem. Eng. J. 2021, 403, 126333.
- X. Cao, Z. Wang, Z. Qiao, S. Zhao, J. Wang, ACS Appl. Mater. Interfaces **2019**, 11, 5306-5315.

- [8] L. Zhai, N. Huang, H. Xu, Q. Chen, D. Jiang, Chem. Commun. 2017, 53, 4242-4245.
- [9] K. Zhang, S. L. Cai, Y. L. Yan, Z. H. He, H.-M. Lin, X. L. Huang, S. R. Zheng, J. Fan, W. G. Zhang, J. Chromatogr. A 2017, 1519, 100–109.
- [10] Y.L. Yan, D. Guo, J.L. Wu, X.H. Tang, J.J. Luo, S.Q. Li, J. Fan, S.R. Zheng, W. G. Zhang, S. L. Cai, J. Chromatogr. A 2022, 1675, 463155-463120.
- [11] X. Han, J. Huang, C. Yuan, Y. Liu, Y. Cui, J. Am. Chem. Soc. 2018, 140, 892-895.
- [12] H. L. Qian, C. X. Yang, X. P. Yan, Chem. Commun. 2018, 54, 11765–11768.
- [13] H. L. Qian, C. X. Yang, X. P. Yan, Nat. Commun. 2016, 7, 12104.
- [14] Z. Alsudairy, N. Brown, A. Campbell, A. Ambus, B. Brown, K. Smith-Petty, X. Li, Mater. Chem. Front. 2023, 21, 5031-5456.
- [15] S. Mondal, B. Mohanty, M. Nurhuda, S. Dalapati, R. Jana, M. Addicoat, A. Datta, B. K. Jena, A. Bhaumik, ACS Catal. 2020, 10, 5623–5630.
- [16] S. Paul, M. Gupta, K. Dey, A. K. Mahato, S. Bag, A. Torris, E. B. Gowd, H. Sajid, M. A. Addicoat, S. Datta, R. Banerjee, Chem. Sci. 2023, 14, 6643-6653.
- [17] H. Li, Q. Pan, Y. Ma, X. Guan, M. Xue, Q. Fang, Y. Yan, V. Valtchev, S. Qiu, J. Am. Chem. Soc. 2016, 138, 14783–14788.
- [18] S. Y. Ding, J. Gao, Q. Wang, Y. Zhang, W. G. Song, C. Y. Su, W. Wang, J. Am. Chem. Soc. 2011, 133, 19816-19822.
- [19] G. Chen, H. H. Lan, S. L. Cai, B. Sun, X. L. Li, Z. H. He, S. R. Zheng, J. Fan, Y. Liu, W. G. Zhang, ACS Appl. Mater. Interfaces 2019, 11, 12830–12837.
- [20] S. Y. Ding, M. Dong, Y. W. Wang, Y. T. Chen, H. Z. Wang, C. Y. Su, W. Wang, J. Am. Chem. Soc. 2016, 138, 3031–3037.
- [21] C. Zhang, S. Zhang, Y. Yan, F. Xia, A. Huang, Y. Xian, ACS Appl. Mater. Interfaces 2017, 9, 13415-13421.
- [22] S. Zhang, Q. Yang, X. Xu, X. Liu, Q. Li, J. Guo, N. Torad, S. M. Alshehri, T. Ahamad, M. S. A. Hossain, Y. V. Kaneti, Y. Yamauchi, Nanoscale 2020, 12, 15611-15619.
- [23] D. M. Li, S. Y. Zhang, J. Y. Wan, W. Q. Zhang, Y. L. Yan, X. H. Tang, S. R. Zheng, S. L. Cai, W. G. Zhang, CrystEngComm **2021**, 23, 3594–3601.
- [24] S. L. Cai, Y. B. Zhang, A. B. Pun, B. He, J. H. Yang, F. M. Toma, I. D. Sharp, O. M. Yaghi, J. Fan, S. R. Zheng, W. G. Zhang, Y. Liu, Chem. Sci. 2014, 5, 4693-
- [25] Q. Hao, C. Zhao, C. Sun, C. Lu, J. Liu, M. Liu, L. J. Wan, D. Wang, J. Am. Chem. Soc. 2018, 140, 12152-12158.
- [26] S. Cai, B. Sun, X. Li, Y. Yan, A. Navarro, A. Garzon-Ruiz, H. Mao, R. Chatterjee, J. Yano, C. Zhu, J. A. Reimer, S. Zheng, J. Fan, W. Zhang, Y. Liu, ACS Appl. Mater. Interfaces 2020, 12, 19054–19061.
- [27] Q. Jiang, Y. Li, X. Zhao, P. Xiong, X. Yu, Y. Xu, L. Chen, J. Mater. Chem. A **2018**, *6*, 17977–17981.
- [28] Z. Cheng, H. Pan, H. Zhong, Z. Xiao, X. Li, R. Wang, Adv. Funct. Mater. 2018, 28, 1707597.
- [29] Y. Song, Q. Sun, B. Aguila, S. Ma, Adv. Sci. 2019, 6, 1801410.
- [30] J. Sun, A. Klechikov, C. Moise, M. Prodana, M. Enachescu, A. V. Talyzin, Angew. Chem. 2018, 130, 1046-1050.
- [31] Y. Liang, L. J. Feng, X. Liu, Y. X. Zhao, Q. Chen, Z. Y. Sui, N. Wang, Chem. Eng. J. 2021, 404, 127095.
- [32] S. P. S. Fernandes, P. Kovar, M. Psenicka, A. M. S. Silva, L. M. Salonen, B. Espina, ACS Appl. Mater. Interfaces **2021**, *13*, 15053–15063.
- [33] G. Y. Lee, J. Lee, H. T. Vo, S. Kim, H. Lee, T. Park, Sci. Rep. 2017, 7, 557.
- [34] Y.Y. Lu, X.L. Wang, L.L. Wang, W. Zhang, J.J. Wei, J.M. Lin, R.S. Zhao, J. Hazard. Mater. 2021, 407, 124782.
- [35] S. Y. Zhang, X. H. Tang, Y. L. Yan, S. Q. Li, S. R. Zheng, J. Fan, X. L. Li, W. G. Zhang, S. L. Cai, ACS Macro Lett. 2021, 10, 1590-1596.
- [36] W. Ji, L. L. Xiao, Y. H. Ling, C. Ching, M. Matsumoto, R. P. B. Damian, E. Helbling, W. R. Dichtel, J. Am. Chem. Soc. 2018, 140, 12677-12681.
- [37] M. S. Lohse, T. Stassin, G. Naudin, S. Ameloot, D. D. Vos, D. D. Medina, T. Bein, Chem. Mater. 2016, 28, 626-631.
- [38] H. L. Qian, Y. Li, X. P. Yan, J. Mater. Chem. A 2018, 6, 17307–17311.
- [39] H. L. Qian, Z. H. Wang, J. Yang, X. P. Yan, Chem. Commun. 2022, 58, 8133-8136.
- [40] E. Dautzenberg, G. N. Li, L. C. P. M. de Smet, ACS Appl. Mater. Interfaces **2023**, *15*, 5118–5127.
- [41] T. Banerjee, F. Haase, S. Trenker, B. P. Biswal, G. Savasci, V. Duppel, I. Moudrakovski, C. Ochsenfeld, B. V. Lotsch, Nat. Commun. 2019, 10, 2689.
- [42] B. Zhang, H. Y. Mao, R. Matheu, J. A. Reimer, S. A. Alshmimri, S. Alshihri, O. M. Yaghi, J. Am. Chem. Soc. 2019, 141, 11420-11424.
- [43] C. Y. Xu, J. Y. Lin, D. Yan, Z. Y. Guo, D. J. Austin, H. B. Zhan, A. Kent, Y. F. Yue, ACS Appl. Nano Mater. 2020, 3, 6416–6422.
- [44] X. H. Tang, Y. X. Yang, X. L. Li, X. J. Wang, D. Guo, S. Y. Zhang, K. Zhang, J. L. Wu, J. Y. Zheng, S. R. Zheng, J. Fan, W. G. Zhang, S. L. Cai, ACS Appl. Mater. Interfaces 2023, 15, 24836-24845.

- [45] Z. Y. Dong, Y. X. Yang, X. T. Cai, X. H. Tang, Y. L. Yan, S. R. Zheng, W. G. Zhang, S. L. Cai, J. Fan, J. Solid State Chem. 2022, 316, 123644.
- [46] Z. F. Pang, T. Y. Zhou, R. R. Liang, Q. Y. Qi, X. Zhao, Chem. Sci. 2017, 8, 3866.
- [47] Y. P. Mo, X. H. Liu, D. Wang, ACS Nano 2017, 11, 11694–11700.
- [48] Z. Q. Zhao, J. W. Zhao, S. M. Zhang, G. Zhang, W. B. Chen, Z. F. Yang, T. Zhang, L. Chen, *Nanoscale* 2021, 13, 19385–19390.
- [49] A. M. Kaczmarek, H. S. Jena, C. Krishnaraj, H. Rijckaert, S. K. P. Veerapandian, A. Meijerink, P. V. D. Voort, Angew. Chem. Int. Ed. 2021, 60, 3727– 3736
- [50] G. Das, F. Benyettou, S. K. Sharma, S. K. Sharama, T. Prakasam, F. Gandara, V. A. de la Pen'-O'Shea, N. Saleh, R. Pasricha, R. Jagannathan, M. A. Olson, A. Trabolsi, Chem. Sci. 2018, 9, 8382–8387.
- [51] C. Krishnaraj, A. M. Kaczmarek, H. S. Jena, K. Leus, N. Chaoui, J. Schmidt, R. Van Deun, P. Van Der Voort, ACS Appl. Mater. Interfaces 2019, 11, 27343–27352.
- [52] X. Wu, X. Han, Y. Liu, Y. Liu, Y. Cui, J. Am. Chem. Soc. 2018, 140, 16124– 16133.
 - [53] Y. Jiang, H. Jung, S. H. Joo, Q. K. Sun, C. Li, H. J. Noh, I. Oh, Y. J. Kim, S. K. Kwak, J. W. Yoo, J. B. Baek, Angew. Chem. Int. Ed. 2021, 60, 17191–17197.
- [54] S. X. Yang, X. Li, Y. Qin, Y. Cheng, W. W. Fan, X. J. Lang, L. Y. Zheng, Q. Cao, ACS Appl. Mater. Interfaces 2021, 13, 29471–29481.
- [55] K. Koner, A. Sadhukhan, S. Karak, H. S. Sasmal, Y. Ogaeri, Y. Nishiyama, S. G. Zhao, M. Položij, A. Kuc, T. Heine, R. Banerjee, *J. Am. Chem. Soc.* 2023, 145, 14475–14483.
- [56] P. Majumder, A. Basak, H. Kuiry, H. S. Sasmal, S. Karak, P. Saha, B. Chandra, S. S. Gupta, R. Banerjee, J. Am. Chem. Soc. 2023, 34, 18855–18864.
- [57] A. S. Eltaweil, H. M. Elshishini, Z. F. Ghatass, G. M. Elsubruiti, *Power Technol.* 2021, 379, 407–416.
- [58] W. T. Gao, B. Mu, Y. F. Zhu, A. Q. Wang, Appl. Clay Sci. 2023, 242, 107003.

- [59] K. Y. Yue, L. Wang, Y. Ma, P. Yang, Y. Q. Zhang, Y. Jiang, B. Tang, *Dalton Trans*. **2019**, *48*, 17763–17769.
- [60] G. P. Zhang, R. Wo, Sun, G, Z. Hao, G. G. Liu, Y. N. Zhang, H. Guo, W. Jiang, *Nanomaterials* 2021, 11, 1917.
- [61] S. F. Lu, Y. J. Wei, S. X. Long, Z. Y. Chen, F. X. Chen, H. R. Lin, J. Y. Lu, ChemistrySelect 2023, 8, e202203621.
- [62] S. Q. Deng, Y. L. Miao, Y. L. Tan, H. N. Fang, Y. T. Li, X. J. Mo, S. L. Cai, J. Fan, W. G. Zhang, S. R. Zheng, *Inorg. Chem.* 2019, 58, 13979–13987.
- [63] W. Jiang, D. Peng, W. R. Cui, R. P. Liang, J. D. Qiu, ACS Omega 2020, 5, 32002–32010.
- [64] Q. B. Liao, C. Ke, X. Huang, G. Y. Zhang, Q. Zhang, Z. W. Zhang, Y. Y. Zhang, Y. Z. Liu, F. Y. Ning, K. Xi, J. Mater. Chem. 2019, 7, 18959–18970.
- [65] S. C. Liu, L. J. Yang, T. Quan, L. L. Deng, D. D. Wang, K. L. Zhang, L. C. Wang, J. J. Wang, F. M. Ke, X. Li, D. Gao, Sep. Purif. Technol. 2022, 288, 120673–120684.
- [66] X. P. Liu, C. L. Hao, L. Cui, Y. J. Wang, Polyhedron 2020, 188, 114685– 114690.
- [67] J. Zhang, F. Li, Q. Sun, Appl. Surf. Sci. 2018, 440, 1219–1226.
- [68] S. Karak, K. Dey, A. Torris, A. Halder, S. Bera, F. Kanheerampockil, R. Banerjee, J. Am. Chem. Soc. 2019, 141, 7572–7581.
- [69] A. K. Mohammed, S. Usgaonkar, F. Kanheerampockil, S. Karak, A. Halder, M. Tharkar, M. Addicoat, T. G. Ajithkumar, R. Banerjee, J. Am. Chem. Soc. 2020, 142, 8252–8261.
- [70] R. Li, X. H. Tang, J. L. Wu, K. Zhang, Q. N. Zhang, J. Q. Wang, J. Y. Zheng, S. R. Zheng, J. Fan, W. G. Zhang, X. L. Li, S. L. Cai, *Chem. Eng. J.* 2023, 464, 142706.

Manuscript received: November 14, 2023 Accepted manuscript online: January 9, 2024 Version of record online: January 18, 2024